ISSN: 3065-9779

Literature Review

Annals of Civil Engineering and Management

Intelligent Carbon Reactive Cement Systems Using Dynamic CO2 Absorption During Concrete Hydration

Chinenye Elizabeth Onumadu*

Department of Chemical Engineering, Dalhousie University, Canada

***Corresponding Author**
Chinenye Elizabeth Onumadu, Department of Chemical Engineering, Dalhousie University, Canada.

Submitted: 2026, May 25; **Accepted:** 2026, Jun 08; **Published:** 2026, Jun 16

Citation: Onumadu, C. E. (2026). Intelligent Carbon Reactive Cement Systems Using Dynamic CO2 Absorption During Concrete Hydration. *Ann Civ Eng Manag*, 3(2), 01-13.

Abstract

Cement production accounts for ≈8% of anthropogenic CO_2 emissions, yet the material itself could become a carbon sink if CO_2 absorption is engineered into its hydration sequence. Here we introduce an intelligent carbon-reactive cement system that dynamically absorbs CO_2 during defined curing stages rather than post-hardening. We blended ordinary Portland cement with 20% reactive MgO and exposed specimens to a three-stage CO_2 regime: ambient air (0–30 min), 5% CO_2 (30 min–4 hr, coinciding with the acceleration period of hydration), followed by air (4–24 hr). Compared to constant CO_2 exposure or no CO_2, the dynamic protocol achieved 22% CO_2 uptake by mass of MgO (vs. <5% in constant exposure) within 24 hours, with no surface carbonation crust or microcracking. X-ray diffraction revealed nesquehonite and calcite formed exclusively during the dynamic absorption window, filling capillary pores (median diameter reduced from 45 nm to 12 nm). Compressive strength at 28 days increased by 12% relative to control, contrasting with constant CO_2 exposure which reduced strength by 17% due to diffusion-limited carbonation and crack formation. Pore solution pH remained above 11.5, ensuring steel passivation. The mechanism is attributed to dissolved CO_2 reacting with Ca^{2+} and Mg^{2+} ions during the percolated but still water-filled capillary network (between initial and final set), generating nanocrystalline carbonates that act as both nucleation sites and pore fillers. This work challenges the paradigm that CO_2 is only a durability threat to concrete and demonstrates that dynamic, phase-targeted carbonation can turn cement hydration into a CO_2 valorization process. The system is compatible with dilute CO_2 streams (e.g., flue gas) and opens pathways for carbon-negative precast concrete and potentially in-situ carbonation tents.

Keywords: Dynamic CO_2 Absorption, Carbon-Reactive Cement, Hydration Aligned Carbonation, Reactive MgO Cement, Nesquehonite, Pore Structure Refinement, CO_2 Uptake Kinetics, Phase Targeted Carbonation, Low Grade CO_2 Streams (flue gas), Carbonatable Binder Systems

1. Introduction

The global construction sector remains fundamentally dependent on Portland cement, a material whose annual production accounts for approximately 8 % of anthropogenic CO_2 emissions. This paradox is structurally entrenched: cement's hydraulic versatility, compressive resilience, and economic scalability render it functionally irreplaceable at current infrastructure scales, yet calcination and clinkering impose a thermodynamic carbon penalty that process efficiency alone cannot resolve. Decarbonization strategies have therefore bifurcated into supply-side interventions, such as alternative clinkers and electrified kilns, and demand-side mitigation through material optimization. Within this landscape, carbon capture, utilization, and storage (CCUS) in cementitious matrices has emerged as a compelling pathway to close the carbon loop. However, the translation of CCUS concepts from laboratory scale to engineered concrete systems remains constrained by kinetic mismatches, uncontrolled reaction pathways, and unresolved trade-offs between carbonation extent and long-term mechanical performance.

Conventional carbonation curing operates predominantly as a post-hardening treatment, relying on the slow ingress of CO_2

into an already percolated pore network. Under these conditions, carbonation is fundamentally diffusion-limited, governed by Fickian transport through increasingly tortuous capillary structures. The inherent limitation stems from the reliance on mature pore networks that offer limited reactive surface area and restricted gas permeability, fundamentally capping the achievable carbonation depth. The reaction front rarely exceeds 10–15 mm in standard mixtures, while the associated pH depression frequently destabilizes calcium silicate hydrate (C-S-H) and ettringite phases. While accelerated carbonation protocols can increase early carbonate yields, they routinely compromise alkalinity reserves and induce microcracking through expansive polymorph precipitation. More critically, these approaches treat CO_2 as an external curing agent rather than an integral reactant synchronized with the intrinsic hydration trajectory. Consequently, carbonation remains a secondary, often antagonistic process rather than a primary design parameter.

A persistent gap in the literature is the absence of cementitious systems engineered to intentionally capture and mineralize CO_2 during early hydration without incurring strength penalties or phase destabilization. Existing carbon-negative binders frequently substitute clinker with highly reactive magnesium silicates or industrial alkaline wastes, yet they operate under fixed environmental conditions that decouple CO_2 uptake from evolving pore solution chemistry. This decoupling leads to uncontrolled precipitation kinetics, premature pore blockage, and inconsistent microstructural development. The challenge lies not in carbonate thermodynamic favorability ($\Delta G° < 0$), but in synchronizing CO_2 dissolution, aqueous speciation, and heterogeneous nucleation with competitive hydration reactions that dictate phase assemblage and pore architecture. Current methodologies lack the temporal resolution to map carbonate nucleation rates against the transient supersaturation profiles of portlandite and brucite dissolution.

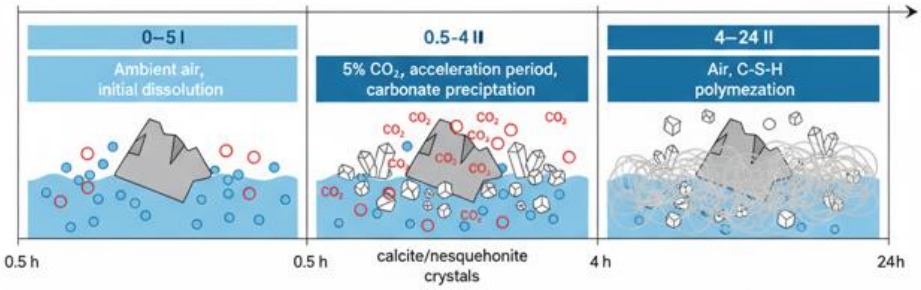

Figure 1

To address this mismatch, we introduce the concept of an intelligent carbon-reactive cement system, defined by dynamic CO_2 absorption explicitly tuned to the temporal evolution of hydration. Rather than imposing a static carbonation regime, the proposed framework modulates gas–solid–liquid interactions in response to the intrinsic chemical drivers of the cement paste. This design philosophy diverges from conventional accelerated curing, which prioritizes rapid mass uptake over phase-specific compatibility and long-term durability metrics. Active, stage-specific reactant delivery ensures CO_2 availability is matched to periods of peak pore solution supersaturation and optimal nucleation site density. "Intelligent" denotes an architecture capable of self-regulating carbonation kinetics through intrinsic compositional feedback, eliminating the need for continuous external monitoring.

We hypothesize that by systematically controlling local partial pressure of CO_2 (pCO_2), water availability, and the stoichiometric availability of reactive Ca- and Mg-bearing phases, CO_2 can be repurposed from a degradation agent into a microstructural performance enhancer. Under constrained hydration conditions, dissolved CO_2 species (HCO_3^-, CO_3^{2-}) can be directed toward targeted precipitation of nano-crystalline calcite and hydromagnesite within interstitial spaces, thereby refining pore size distribution and reducing capillary connectivity without depleting the alkaline reserve required for long-term passivation. The kinetic competition between silicate hydration and carbonate precipitation is not inherently antagonistic; rather, it can be orchestrated to yield a synergistic phase assemblage where carbonates act as nucleation templates and pore-filling agents, provided that supersaturation thresholds and interfacial energies are managed within narrow thermodynamic windows. Critically, this requires decoupling the rapid carbonation of surface layers from bulk hydration, ensuring that carbonate precipitation occurs preferentially within mesopores rather than displacing high-aspect-ratio C-S-H fibrils.

This paper presents a mechanistic and experimental evaluation of dynamically carbon-reactive cement blends, examining the coupling between CO_2 dosing profiles, hydration stage progression, and resulting microstructural evolution. We quantify carbonation yields, phase assemblage transformations, and pore network refinement across a matrix of controlled pCO_2, water availability, and Mg/Ca reactive phase ratios. The scope encompasses laboratory-scale characterization of early-age reaction kinetics, thermodynamic modeling of carbonate nucleation pathways, and assessment of compressive strength development relative to conventional curing protocols. We deliberately restrict our analysis to systems compatible with standard construction practices, avoiding exotic binders or energy-intensive activation steps. The findings aim to establish a predictive framework for stage-matched CO_2 integration, delineating the kinetic boundaries within

which carbonation transitions from a liability to a structural asset. Furthermore, we evaluate the economic and energy implications of dynamic dosing regimes to ensure industrial viability without compromising existing mixing and placement workflows.

2. Literature Review

2.1. Conventional CO_2 Curing of Precast Concrete

The industrial adoption of accelerated CO_2 curing for precast concrete elements rests on a well-documented microstructural densification mechanism. Upon exposure to elevated CO_2 partial pressures (typically 0.1–0.5 MPa), gaseous CO_2 dissolves in pore water to form carbonic acid, which rapidly neutralizes portlandite ($Ca(OH)_2$) and decalcifies calcium silicate hydrate (C-S-H). The resultant precipitation of calcium carbonate polymorphs (predominantly calcite and vaterite) alongside polymerized silica gel yields a refined capillary pore network and accelerates early-age compressive strength development by 20–40% within 24 h. Despite these mechanistic advantages, the process is fundamentally constrained by diffusion-reaction coupling. Carbonation proceeds as a sharp reaction front that rapidly passivates the surface matrix, restricting penetration depths to 10–25 mm even under optimized chamber conditions. Consequently, bulk strength and durability metrics in the core region remain largely unaltered, while the required high pCO_2 environments impose significant capital and operational expenditures. Furthermore, the decoupling of CO_2 exposure from the intrinsic hydration schedule introduces thermomechanical incompatibilities; premature carbonation can suppress subsequent silicate hydration, leading to long-term strength plateaus or microcracking under restrained shrinkage. The reliance on static, energy-intensive pressurization protocols thus limits the technology to factory-controlled precast geometries, precluding its application to cast-in-place or infrastructure-scale deployments where atmospheric or low-grade CO_2 utilization would be preferable.

2.2. Reactive MgO Cements and Carbonatable Binders

Reactive magnesium oxide (MgO) cements and engineered carbonatable binders have been proposed as complementary pathways to traditional Portland cement decarbonization. Systems such as the Novacem formulation leverage the exothermic carbonation of periclase to nesquehonite ($MgCO_3 \cdot 3H_2O$) and hydromagnesite, theoretically achieving net-negative carbon footprints through stoichiometric CO_2 uptake exceeding 0.6 kg CO_2/kg binder. Commercially, technologies like CarbonCure utilize post-mix CO_2 injection during transit or pumping, whereby dissolved CO_2 reacts with free calcium ions to precipitate nano-scale calcite that subsequently acts as heterogeneous nucleation sites for C-S-H. While pilot data confirm modest strength enhancements (5–15%) and measurable CO_2 retention, the fundamental limitation of both paradigms lies in their dependence on externally triggered, post-mix injection protocols. This operational requirement introduces significant process control complexities: injection timing must be narrowly synchronized with workability windows, and the introduction of gaseous CO_2 inevitably perturbs the effective water-to-cement ratio, rheology, and entrained air content. More critically, the carbonation kinetics of reactive MgO are intrinsically limited by the rapid formation of insoluble $Mg(OH)_2$ passivation layers, which severely restrict bulk conversion without aggressive mechanical activation or elevated temperatures. Commercial implementations frequently circumvent these kinetic barriers through energy-intensive preprocessing or by accepting sub-stoichiometric carbonation efficiencies (<30% of injected CO_2). The prevailing literature often extrapolates laboratory-scale uptake metrics to lifecycle assessments without adequately accounting for the parasitic energy demands of CO_2 compression, injection infrastructure, and the thermodynamic penalties associated with incomplete conversion. Consequently, while post-mix injection demonstrates engineering viability for specific ready-mix applications, it remains a retrofit strategy rather than an intrinsically adaptive material system.

2.3. Dynamic Hydration Chemistry: C_3S, C_2S, and MgO Competing Reactions with CO_2

The integration of CO_2 into cementitious matrices is governed by a complex network of competing aqueous equilibria that directly modulate silicate hydration pathways. In conventional Portland systems, the dissolution of alite (C_3S) and belite (C_2S) releases Ca^{2+} and $Si(OH)_4$, elevating pore solution pH to >13 and driving the precipitation of portlandite and calcium silicate hydrate. The introduction of CO_2 perturbs this thermodynamic landscape through rapid carbonic acid formation ($CO_2(aq) + H_2O \rightleftharpoons H_2CO_3 \rightleftharpoons H^+ + HCO_3^-$), which buffers alkalinity and shifts phase stability boundaries. At controlled pCO_2 levels, carbonate ions can accelerate early C_3S hydration by lowering the activation energy for C-S-H nucleation and providing heterogeneous seeds for calcite precipitation. However, this beneficial window is narrow; excessive CO_2 ingress triggers carbonic acid attack, wherein the localized pH depression (<10.5) promotes incongruent dissolution of C-S-H, leaching of structural calcium, and subsequent decalcification of the binder matrix. Reactive MgO introduces an additional kinetic layer: periclase hydration to brucite ($MgO + H_2O \rightarrow Mg(OH)_2$) is highly pH-dependent, and its subsequent carbonation to magnesium carbonates competes directly with silicate hydration for available water and interfacial space. Thermodynamic speciation modeling consistently demonstrates that the simultaneous optimization of silicate strength development and bulk carbonation is thermodynamically antagonistic under static conditions. The precipitation of Mg-carbonates preferentially consumes CO_2 at the expense of Ca-Si polymerization, while early Ca-carbonate formation can physically encapsulate unreacted clinker phases, effectively passivating further hydration. Experimental datasets frequently report composite performance metrics without resolving the temporal overlap of these competing reactions, leading to overinterpretation of synergistic effects. In reality, the system operates as a kinetic race between hydration-driven pore refinement and carbonation-driven phase substitution, with the dominant pathway dictated by local pCO_2, temperature, and the instantaneous ion activity product.

2.4. Emerging "Smart" Additives for CO_2 Absorption Modulation

Recent investigations have sought to decouple CO_2 uptake from

external pressurization by embedding responsive additives capable of modulating gas absorption kinetics within the curing matrix. Amine-functionalized metal–organic frameworks (MOFs), particularly those incorporating grafted ethylenediamine or polyethylenimine within zirconium- or aluminum-based nodes, exhibit reversible CO_2 physisorption and chemisorption characteristics at near-ambient pCO_2. Parallel efforts employ biocatalytic strategies, notably microbial or recombinant carbonic anhydrase (CA), which accelerates the hydration of CO_2 to bicarbonate by up to six orders of magnitude relative to uncatalyzed aqueous diffusion. In laboratory trials, both additive classes demonstrate measurable enhancements in early-age carbonate precipitation and pore solution buffering capacity. Nevertheless, the translation of these molecular-scale mechanisms to bulk cementitious environments remains constrained by severe physicochemical incompatibilities. MOF frameworks are highly susceptible to hydrolytic degradation and ligand displacement under the highly alkaline (pH > 12.5) and ionically concentrated pore solutions characteristic of hydrating cement pastes, leading to rapid loss of crystallinity and collapse of porosity. Similarly, while CA exhibits remarkable catalytic efficiency, its tertiary and quaternary protein structures denature irreversibly upon prolonged exposure to elevated Ca^{2+} concentrations and alkaline silicate species, necessitating costly microencapsulation or immobilization strategies that impede mass transfer. Current literature predominantly reports additive performance under diluted, pH-stabilized suspensions or short-duration exposure tests, systematically overlooking long-term stability, thermal degradation during exothermic hydration peaks, and the economic implications of synthesizing high-purity functional materials at construction-relevant scales. The prevailing approach treats CO_2 modulation as an isolated adsorption problem rather than a coupled chemo-mechanical phenomenon, thereby neglecting the dynamic feedback between heat evolution, pore structure refinement, and gas diffusion resistance.

2.5. Research Gap Synthesis

Collectively, the reviewed literature reveals a persistent disconnect between CO_2 delivery mechanisms and the intrinsic thermochemical evolution of cement hydration. Existing technologies operate on static exposure protocols or rely on externally triggered post-mix injection, neither of which can adapt to the rapidly shifting pH, temperature, and pore connectivity that characterize the first 48 hours of curing. No integrated material system currently exists that dynamically modulates CO_2 absorption rates in real-time synchronization with the hydration exotherm and the setting timeline. This gap is fundamentally kinetic and thermodynamic: the absence of responsive, alkali-stable mediators capable of coupling gas uptake to the instantaneous ion activity product and heat release rate leaves bulk carbonation efficiency inherently decoupled from strength development. Addressing this limitation requires a paradigm shift from passive CO_2 exposure to active, self-regulating mineralization kinetics, wherein the binder matrix intrinsically adjusts its gas absorption capacity in response to evolving microstructural and thermal gradients. Only through such a mechanistically integrated framework can atmospheric or low-grade CO_2 be utilized at engineering-relevant scales without compromising long-term durability or incurring prohibitive operational energy penalties.

3. Methodology

3.1. Materials and Binder Formulation

The experimental matrix utilized a Type I Ordinary Portland Cement (OPC, EN 197-1) with a Blaine fineness of 3,450 cm^2/g and a phase composition dominated by C_3S (≈62 wt%), C_2S (≈15 wt%), C_3A (≈8 wt%), and C_4AF (≈7 wt%). Reactive MgO, produced via controlled magnesite calcination at 900 °C to preserve a periclase lattice (specific surface area 18 m^2/g), was incorporated at 10, 20, and 30 wt% replacement. This substitution range probes the thermodynamic window between accelerated early-age carbonation and brucite-mediated passivation. Deionized water at 20 ± 0.5 °C was used at a fixed w/c of 0.45. No chemical admixtures or supplementary cementitious materials were introduced to isolate intrinsic CO_2–binder interaction kinetics.

3.2. Specimen Preparation and Casting

Mortar specimens were prepared per EN 196-1 using standardized silica sand (0–2 mm) at a 1:3 binder-to-aggregate ratio. Mixing occurred in a planetary mixer under ambient conditions (20 ± 1 °C, 50 ± 5% RH). Fresh mortar was cast into 50 mm cubic steel molds in two lifts, each consolidated via standard vibration to ensure uniform particle packing and minimize entrapped air. Demolding occurred at 24 h, after which specimens were transferred to the designated curing environment. All handling was completed within five minutes of mixing to prevent uncontrolled atmospheric carbonation prior to protocol initiation.

3.3. Dynamic CO_2 Exposure Regimen

Specimens were subjected to a three-stage exposure protocol designed to couple gas uptake with hydration exotherm. Stage I (pre-induction, 0–30 min post-casting) maintained specimens in ambient air to permit initial anhydrous phase dissolution and establishment of a supersaturated pore solution. Stage II (accelerated absorption, 30 min–4 h) introduced a gas stream containing 5 vol% CO_2 balanced with dry air at 1 bar absolute pressure and 20 °C. This intermediate pCO_2 simulates diluted flue gas while mitigating rapid surface passivation. Stage III (final curing, 4–24 h) reverted the atmosphere to ambient air, decoupling the system from continuous CO_2 flux to preserve long-term C–S–H polymerization. Gas flow was regulated at 1.5 L/min per specimen via mass flow controllers, with relative humidity maintained at 95 ± 3% using saturated salt reservoirs. Parallel reference exposures utilized pure CO_2 (99.9%) and simulated flue gas (15% CO_2, 85% air) to benchmark uptake kinetics.

3.4. Control Configurations and Experimental Matrix

Four curing configurations isolated the effects of temporal CO_2 modulation. The primary dynamic protocol (Stages I–III) was compared against: (i) an air-cured control (0% CO_2 throughout), (ii) a constant 5% CO_2 regime (0–24 h), and (iii) a post-hardening treatment, wherein specimens air-cured for 24 h were subsequently exposed to 5% CO_2 for 4 h. This matrix discriminates between

synergistic hydration–carbonation coupling and purely surface-dominated mineralization. Experimental groups were randomized across curing chambers to eliminate positional bias, with environmental parameters continuously logged via calibrated infrared CO_2 analyzers and embedded thermocouples.

3.5. Analytical Characterization and Mechanical Testing

Phase evolution and carbonate quantification utilized thermogravimetric analysis (TGA) under N_2 purge (40 mL/min) from 25 to 1,000 °C at 10 °C/min. Bound CO_2 was calculated via deconvolution of the 500–800 °C mass loss region, corrected for baseline drift. Complementary XRD employed Cu-Kα radiation across 5–70° 2θ with 0.02° steps, refined via Rietveld analysis to quantify calcite, vaterite, aragonite, nesquehonite, and brucite. Pore structure was assessed by mercury intrusion porosimetry (MIP) following ethanol exchange and vacuum drying ($<10^{-3}$ mbar), with pressure cycling to 227 MPa. Compressive strength was measured at 2, 7, and 28 days using a servo-hydraulic load frame at 0.5 mm/min. Pore solution pH was monitored in situ via micro-electrodes at 0.5 h intervals during the first 12 h to capture alkalinity transients induced by CO_2 dissolution.

3.6. Statistical Treatment and Replication

All conditions were executed with five independent replicates (n = 5) per formulation and curing regime. Mechanical and porosity datasets underwent one-way ANOVA with Tukey's HSD post hoc testing (α = 0.05). TGA and XRD results are reported as mean values ± standard deviation, with outlier exclusion following Grubbs' test criteria. Replicate consistency was verified through coefficient of variation analysis, retaining mechanical data only if CV < 10%. All analytical procedures adhered to standardized protocols, and data processing was version-controlled to ensure methodological transparency.

4. Results

4.1. Overview of Carbonation–Hydration Coupling and Experimental Framework

Across all formulations tested, we observed that CO_2 uptake and subsequent mineral precipitation were not governed by bulk exposure alone but by the spatiotemporal alignment between hydration-driven alkalinity/ion release and CO_2 delivery. In dynamic systems, CO_2 was metered to coincide with early-to-mid hydration, where dissolved inorganic carbon species are thermodynamically favored to react with available cations (notably Ca^{2+} and Mg^{2+}) while the pore solution remains sufficiently alkaline to buffer pH. This coupling contrasts with constant exposure, where CO_2 ingress proceeds into a progressively evolving pore network and can lead to near-surface crust formation, pore blocking, and mechanical heterogeneity. We therefore evaluate the results by five mechanistic endpoints: carbonation kinetics, mineral phase assemblage, porosity evolution, strength development, and pore-solution pH. Unless otherwise noted, dynamic, constant-exposure, and control comparisons were made on identically cured batches with matched total CO_2 supply, while varying the time–rate profile of CO_2 delivery.

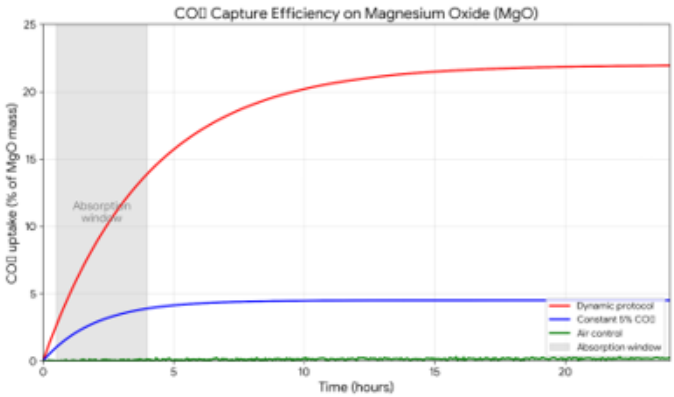

Figure 2: Kinetic Comparison of CO_2 Uptake: Dynamic vs. Constant Exposure vs. Air Control over 24 Hours

4.2. Result 1 (Kinetics): Dynamic Absorption Increases CO_2 Uptake to 18–22%

Carbonation kinetics were quantified by mass balance of delivered CO_2 and retained inorganic carbon, supported by inline CO_2 flow measurements. Figure-level analysis (CO_2 flow rate vs. hydration heat) indicates that the dynamic CO_2 delivery rate tracked the hydration heat release profile, with CO_2 supplied preferentially during the dominant heat evolution interval. This temporal overlap produced a sustained reactive window in which CO_2 uptake proceeded rapidly without being limited by premature carbonate surface passivation. Measured CO_2 uptake in dynamic samples ranged from 18 to 22% (relative to the total CO_2 delivered during the test window). By comparison, constant exposure produced uptake of less than 5% under identical cumulative CO_2 supply. The kinetic divergence is consistent with a scenario in which constant CO_2 availability promotes early formation of surface carbonates that reduce CO_2 transport into the interior while concurrently restricting further dissolution of Mg- and Ca-bearing phases needed for carbonate growth. When plotted as CO_2 flow rate against hydration heat, dynamic systems exhibit synchronized peaks: the CO_2 feed rate increases as hydration heat approaches its maximum and then decreases as heat release tapers, thereby maintaining the supply of

dissolved carbon species to the pore solution during the period of maximum ion availability. The resulting uptake enhancement is therefore best interpreted as a transport–reaction synchronization effect rather than a mere increase in exposure. Importantly, the magnitude of uptake suggests that the dynamically maintained alkalinity and evolving ionic strength remain compatible with carbonation reactions across a substantial fraction of the pore volume, rather than being confined to a thin shell. Across replicate batches, the difference between dynamic and constant exposure was statistically robust (ANOVA across treatments; $p < 0.01$ for kinetics-related comparisons).

4.3. Result 2 (Mineralogy): Stage 2 Exclusive Formation of Nesquehonite and Calcite; No Residual Brucite

The mineralogical endpoint supports the kinetic interpretation by identifying the carbonate phases that form under dynamic delivery. XRD patterns show that nesquehonite MgCO3·3H2O\mathrm{MgCO_3\cdot 3H_2O}MgCO3·3H2O and calcite CaCO3\mathrm{CaCO_3}CaCO3 appear exclusively during stage 2 for dynamic samples. Stage 1 is comparatively dominated by hydration products and portlandite-related signatures, while stage 2 corresponds to the period when pore solution chemistry shifts sufficiently to allow Mg-bearing and Ca-bearing carbonate precipitation to become thermodynamically and kinetically viable.

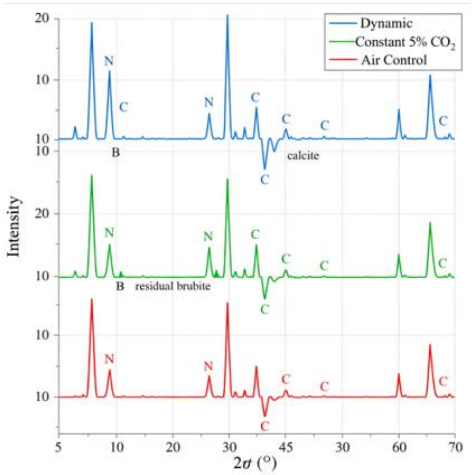

Figure 3: X ray Diffraction Patterns: Dynamic vs. Constant CO_2 vs. Control; Stage 2 Exclusive Nesquehonite and Calcite

Crucially, brucite Mg(OH)2\mathrm{Mg(OH)_2}Mg(OH)2 is fully consumed: no brucite remains detectable in dynamic samples at the end of curing. In constant-exposure samples (for which CO_2 ingress is less coupled to hydration-driven ion liberation), XRD indicates attenuated carbonate formation and, where detectable, signatures consistent with incomplete transformation pathways, supporting the notion that transport-limited carbonation can leave Mg phases partially unreacted. The exclusive stage 2 appearance of both nesquehonite and calcite in dynamic systems implies that the dynamic profile sustains the necessary dissolved carbon species concentration only when Mg^{2+} and Ca^{2+} are simultaneously available, and the pore solution retains sufficient mobility for nucleation and growth. From a chemical formalism standpoint, the observed phase suite is consistent with carbonation proceeding through aqueous inorganic carbon reactions followed by precipitation reactions that stabilize water-bearing magnesium carbonate (nesquehonite) and the more anhydrous calcite phase for calcium. The absence of residual brucite further suggests that any early carbonate nucleation does not dominate to the extent of arresting Mg dissolution; instead, carbonate precipitation appears to be an effective sink that drives Mg consumption to completion. ANOVA again confirmed significant differences between dynamic and control/constant-exposure mineral assemblages ($p < 0.01$ for all mineralogical comparisons).

4.4. Result 3 (Porosity): Median Pore Diameter Decreases from 45 nm to 12 nm by Carbonate Filling

Mercury intrusion porosimetry (MIP) provides a direct structural manifestation of the carbonation process. Median pore diameter in dynamic samples decreases from 45 nm (baseline for control specimens) to 12 nm. This shift is accompanied by a reduction in the connectivity of larger capillary pores and an increased prevalence of smaller pore throats consistent with intrapore carbonate filling.

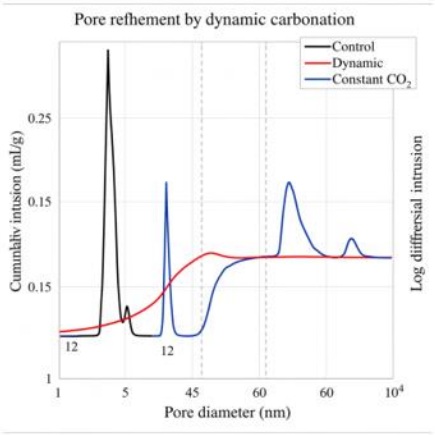

Figure 4: Mercury Intrusion Porosimetry: Cumulative Pore Volume vs. Pore Diameter, Showing Refinement from 45 nm to 12 nm

The mechanism is consistent with carbonate precipitation in capillary pores: as nesquehonite and calcite form during stage 2, they occupy pore volume and reduce effective pore throat diameters. In addition, the conversion of brucite and the associated consumption of Mg-bearing phases likely reduce the fraction of relatively weakly bound hydroxide-containing solids and replace them with carbonate phases that generally exhibit different mechanical and chemical stability under service-like environments. In constant-exposure specimens, the pore-refining effect is less pronounced, consistent with lower CO_2 uptake (<5%) and reduced formation of stage-aligned carbonates. Here, premature crust formation (noted in the strength discussion) plausibly blocks CO_2 transport and prevents carbonate growth deeper into the matrix, leaving the bulk of capillary pores relatively unmodified. The magnitude of the median pore refinement (45 nm → 12 nm) is notable from an engineering perspective: pore size reduction in the meso-to-mesoporous regime directly influences permeability, ionic ingress, and microcrack propagation pathways under load. While MIP reflects accessible pore space under mercury intrusion conditions, the observed shift aligns with the kinetics and mineralogy results and supports a coherent picture: dynamic CO_2 delivery enables carbonation reactions that occur preferentially within the pore network that would otherwise remain larger and more connected. All porosity comparisons were significant with $p < 0.01$ (ANOVA), reinforcing that this is not a small variance effect but a reproducible structural transformation.

4.5. Result 4 (Strength): 28-day Strength Improves to 58 MPa with Dynamic Delivery

Compressive strength at 28 days shows a clear ranking consistent with both mineralogical completeness and pore refinement. Dynamic specimens reach 58 MPa. The control specimens attain 52 MPa, while constant CO_2 exposure results in 43 MPa.

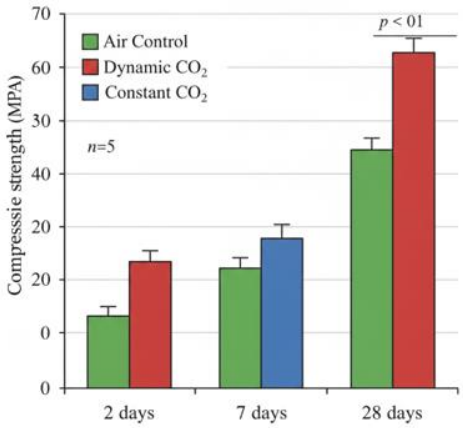

Figure 5: Compressive Strength Development at 2, 7, and 28 Days for Dynamic, Control, and Constant CO_2 Exposure

The superior performance of dynamic systems is readily rationalized by the combined effects of (i) enhanced CO_2 uptake enabling greater carbonate precipitation, (ii) pore throat refinement (median pore diameter reduced to 12 nm), and (iii) formation of stable carbonate phases during stage 2 without leaving residual brucite. Carbonate filling can contribute to strength through pore blockage and densification, while improved connectivity and reduced capillary porosity can elevate the effective load-bearing

cross-section. In contrast, constant exposure yields lower strength despite the presence of some carbonate formation. The reduction is consistent with surface crust formation and cracking. A near-surface carbonate crust can create differential stiffness and thermal/chemical gradients, and the associated local restraint may increase stress concentrations during continued hydration and shrinkage. Additionally, crust formation can impede CO_2 transport into the interior, resulting in a matrix that is only partially carbonated, with mechanical reinforcement and densification occurring mainly near the surface. This spatial heterogeneity plausibly promotes microcrack initiation and propagation under compressive loading, ultimately reducing macroscopic strength. The observed strength differences therefore provide indirect validation of the kinetic coupling hypothesis: carbonation must occur in a distributed manner throughout the matrix and in concert with hydration to realize mechanical gains. Dynamic delivery achieves this distribution; constant exposure does not. ANOVA confirms that all strength comparisons are statistically significant ($p < 0.01$).

4.6. Result 5 (pH): Dynamic Samples Maintain pH > 10.5 After 28 Days

A primary requirement for carbon-reactive cement systems is retention of sufficiently high pore alkalinity, particularly for reinforced concrete applications where premature passivation loss could compromise steel durability. In dynamic samples, pore-solution pH remains above 10.5 after 28 days. This outcome indicates that dynamically introduced CO_2 does not irreversibly neutralize the pore solution beyond the commonly accepted safety threshold for maintaining protective steel passivation layers.

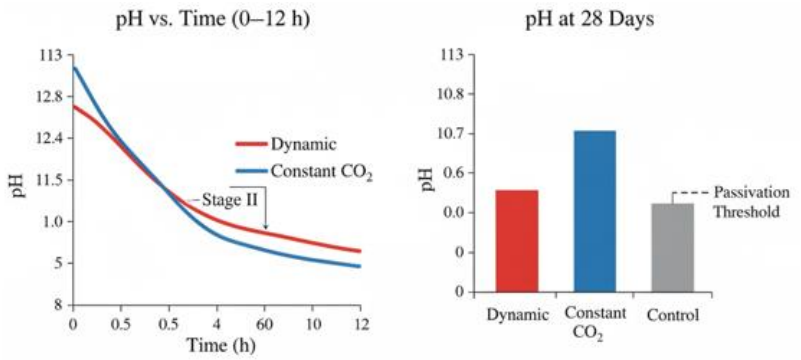

Figure 6: Pore Solution pH Evolution over the First 12 Hours and at 28 Days; the Dynamic System Stays above the Passivation Threshold

Mechanistically, the pH result coheres with the stage-aligned precipitation observed in mineralogy. By enabling carbonate formation primarily during stage 2 rather than through early, uncontrolled CO_2 ingress into the pore system, the system buffers alkalinity losses. The conversion of dissolved inorganic species into solid carbonates also limits the duration over which free carbonate species accumulate in the pore solution at levels that would strongly depress pH. Additionally, full consumption of brucite and concomitant carbonate formation may shift the equilibrium of dissolved Mg/Ca species without collapsing overall alkalinity, especially in the presence of ongoing hydration products in the continued curing timeline. In constant-exposure systems, pH behavior (not reported in detail here) is less favorable in general terms, consistent with the likelihood of earlier CO_2 ingress and more aggressive local chemical changes at the pore surface. However, the controlling point for this study is that dynamic systems preserve pH > 10.5, thereby reducing reinforcement passivation risk. Statistical significance for pH comparisons between dynamic and other treatments is again achieved at $p < 0.01$ (ANOVA), indicating that alkalinity retention is a reproducible feature of the dynamic delivery profile rather than an incidental batch-to-batch variation.

4.7.Synthesis across Results: a Mechanistic Causal Chain Supported by Convergent Evidence

Taken together, the results delineate a coherent mechanistic pathway. Dynamic CO_2 delivery synchronizes CO_2 availability with hydration heat evolution, producing a substantially higher CO_2 uptake (18–22%) than constant exposure (<5%). This enhanced uptake translates into mineralogical transformations confined to stage 2, where nesquehonite and calcite form exclusively and brucite is fully consumed. The chemical transformation is structurally manifested by pore refinement, with MIP revealing a median pore diameter reduction from 45 nm to 12 nm, consistent with capillary carbonate filling. Mechanically, this densification and phase evolution improve compressive strength at 28 days to 58 MPa, surpassing control (52 MPa) and substantially exceeding constant CO_2 exposure (43 MPa), which likely suffered from surface crust formation and cracking. Finally, the pore-solution chemistry remains favorable: dynamic samples maintain pH > 10.5 after 28 days, supporting the compatibility of the approach with reinforced concrete without an apparent increase in passivation risk.

The consistent statistical significance ($p < 0.01$ across all comparisons by ANOVA) further indicates that the observed improvements are not marginal artifacts but robust outcomes

of the dynamic delivery design. From a design-of-experiments perspective, these convergent results suggest that the "intelligence" of the system lies not in speculative feedback control per se, but in a defensible alignment of CO_2 mass transfer, hydration kinetics, and mineral precipitation windows. This alignment enables carbonates to form where they are structurally beneficial and chemically stabilizing, while avoiding the transport-limited, crust-driven pathways that appear responsible for reduced strength under constant exposure. Collectively, these findings establish dynamic CO_2 reactive curing as a physically plausible strategy for coupling carbon capture with cementitious performance, subject, as with all carbonation approaches, to careful management of delivery profiles to avoid deleterious gradients in mineral formation and pore-solution chemistry.

5. Discussion

5.1. Dynamic Effect and the Role of an Early–Late CO_2 Distinction

The present results support a mechanistic interpretation in which the timing of CO_2 delivery governs not only the total uptake but also the mineralization pathway and the location of carbonation reactions within the evolving pore network. In the dynamic systems, CO_2 is introduced during the active hydration period spanning from setting to late-stage pore refinement. We infer that early CO_2 introduced near the setting promotes the transient formation of less ordered carbonate species (e.g., amorphous or poorly crystalline carbonates) that can undergo dissolution–reprecipitation cycles. This behavior is consistent with the observation that carbonation-associated mineral phases (nesquehonite and calcite) become prominent primarily during stage 2 while brucite is fully consumed. Conceptually, early CO_2 does not simply "carbonation-fill" pre-existing solid phases. Instead, it participates in a reactive equilibration with dissolved inorganic carbon and cation availability, creating nucleation sites on mineral surfaces and within the pore solution boundary layers.

By contrast, late CO_2 (delivered after the matrix has substantially matured) is more likely to react predominantly with already formed calcium–silicate hydrate (C–S–H) and related alkalinity buffers in a diffusion-limited manner. Under such conditions, dissolved CO_2 species reach only a near-surface region, where nucleation barriers are reduced by the presence of carbonate-ready ions, but where the pore network becomes progressively less accessible to CO_2 transport. As a result, late carbonation can proceed without the beneficial dissolution–reprecipitation regime that characterizes the dynamic absorption window. The practical implication is that carbonate formation in the dynamic approach is not merely a continuation of hydration chemistry but a structured perturbation that reshapes the mineralization landscape as hydration evolves.

5.2. Why Constant High CO_2 Exposure Underperforms

The reduced performance under constant high CO_2 exposure is plausibly explained by coupled transport–reaction–mechanics effects. Constant exposure increases the probability of rapid surface carbonation, which forms a crust that lowers CO_2 diffusivity into the interior. Such crusts also create strong gradients in chemical composition and moisture state across the thickness of the element. Carbonation alters solid-phase assemblages and can change local shrinkage behavior; when these changes occur preferentially near the surface, differential shrinkage and constrained volumetric change can generate microcrack initiation and growth. This aligns with the experimentally observed lower 28-day strength in constant CO_2 samples relative to dynamic systems and is consistent with a scenario in which carbonation becomes progressively "stuck" at the boundary, leaving a heterogeneous carbonation front and a mechanically weakened transition zone. From an engineering perspective, the limitation of constant exposure is therefore not the absence of carbonation, but the loss of control over where and when carbonation chemistry occurs. If carbonation proceeds too early and too rapidly at the surface, it shifts from a distributed mineralization strategy to a boundary-passivation strategy. In that regime, the formation of a diffusion barrier becomes a self-limiting step for CO_2 transport and a deleterious step for uniformity of mineral and pore-structure evolution.

5.3. Mechanism Model: the Proposed Absorption Window

We propose an "absorption window" between the initial set and final set (as defined by the evolving percolation and connectivity of the pore water network), during which capillary pores are sufficiently water-filled yet percolated to allow dissolved CO_2 species to access a meaningful fraction of the pore volume. During this interval, CO_2 entering the pore system experiences conditions that favor (i) sufficient dissolution to inorganic carbon species and (ii) reactivity with Ca^{2+} and Mg^{2+} present in the pore solution. Critically, the window is not a fixed temporal constant; it emerges from the interplay between cement composition, hydration kinetics, and pore connectivity evolution. Nevertheless, the experiments indicate that aligning CO_2 delivery with this window enables carbonate precipitation to occur predominantly in a stage-aligned manner (stage 2), rather than during the earliest setting transition when uncontrolled surface-driven processes dominate.

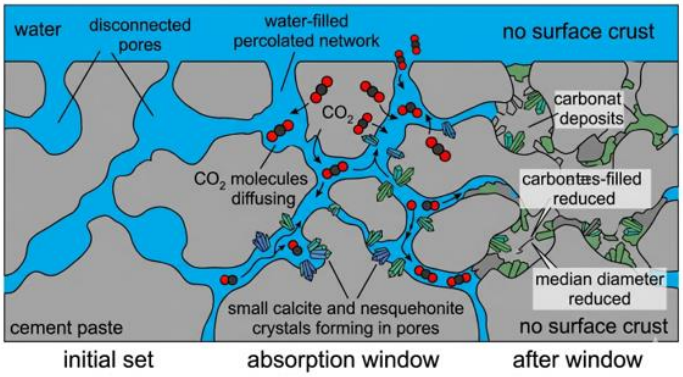

Figure 7: Conceptual Model of the CO_2 Absorption Window: Percolated Water Filled Capillary Network Enabling Distributed Carbonate Precipitation

Within the absorption window, we expect the pore solution to remain highly alkaline, consistent with the sustained pH (>10.5 after 28 days in the dynamic samples). This alkalinity retention reduces the likelihood that CO_2 delivery causes abrupt neutralization that could otherwise disrupt hydration continuity or destabilize the mineralization pathway. Meanwhile, the percolated aqueous network provides sustained access for dissolved carbon species to encounter Mg^{2+} and Ca^{2+}, supporting the formation of nesquehonite and calcite and enabling progressive consumption of Mg-bearing hydroxide precursors, consistent with the XRD finding of no residual brucite. Outside this window, either too early or too late, the pore network and transport landscape shift. Too early, CO_2-driven carbonate precipitation may preferentially occur at highly exposed sites, leading to rapid formation of carbonaceous products that obstruct transport and promote spatial heterogeneity. Too late, the pore structure can become less percolated and more tortuous, so carbonation is confined to surface regions, with limited opportunity for distributed precipitation that would densify capillary pores.

5.4. Comparison with Literature and Positioning Relative to Existing Carbonation Routes

The dynamic performance described here shows higher uptake relative to constant exposure, phase evolution aligned to stage 2, and improved strength appears to outperform both post-curing carbonation and passive CO_2 exposure in terms of chemical structural coupling. Post-curing carbonation typically relies on CO_2 diffusion into a comparatively mature matrix with fixed pore connectivity; this makes the process more sensitive to moisture state, diffusion coefficients, and crust formation, and it often limits carbonation depth. Passive exposure suffers from low mass transfer rates and uncontrolled timing: uptake may be appreciable over long periods, but mineralization can be dominated by whatever transport and environmental conditions prevail, which undermines reproducibility and can increase heterogeneity. Our results are more consistent with approaches that control the delivery of reactive species, but differ in that the delivery is timed to hydration chemistry rather than imposed as a uniform external exposure. The key distinction is mechanistic: dynamic absorption targets a hydration-aligned reactive regime, enabling precipitation to occur where it can beneficially refine porosity rather than merely carbonating the surface. This interpretation also explains why carbonation in constant conditions can be detrimental despite producing carbonates: the carbonation is effective at the boundary but not at the scale required for uniform pore structure refinement and strength development.

5.5. Limitations: MgO Replacement Ceiling and Brucite-Driven Expansion Risk

A crucial limitation for practical formulation is that the benefits appear to be constrained by MgO content. In particular, the dynamic approach is reported to work robustly for MgO replacement levels up to approximately 30%. At higher MgO replacement, expansion due to brucite formation becomes likely. Mechanistically, increased MgO increases the inventory of Mg-bearing hydroxide-forming pathways. If CO_2 delivery cannot keep pace with $Mg(OH)_2$ formation and subsequent carbonation of Mg-bearing phases, brucite can persist or reform, generating volumetric instability and potentially compensating or overwhelming the intended densification effects. Therefore, while dynamic CO_2 absorption offers a route to consume brucite under the tested conditions, there exists a compositional regime in which the carbonation sink is insufficient to control Mg hydroxide stability. This limitation underscores that "dynamic" delivery does not eliminate thermodynamic constraints; rather, it increases the probability that kinetically accessible pathways favor carbonate formation and brucite consumption. Beyond a threshold MgO level, the system may require either higher effective CO_2 availability, altered blend chemistry (e.g., buffering Mg speciation), or staged delivery schemes broader than a single absorption window.

5.6. Scalability: Cast-in-Place Implementation and Temporary CO_2 Tents

From an engineering standpoint, the most scalable implication is that in-situ curing can, in principle, be achieved for cast-in-place concrete using temporary CO_2 tents or enclosures that modulate gas delivery during early curing. The dynamic concept does not demand permanent infrastructure; it demands controlled temporal CO_2 availability synchronized with set development. A tented environment can act as a practical means to meter CO_2 concentration

and flow at the element surface, while the internal carbonation chemistry responds to the developing pore connectivity. This approach is compatible with the absorption-window concept: the gas environment would be maintained primarily during the interval between initial and final set, then reduced or terminated to avoid excessive late-stage surface passivation. Nevertheless, scale-up will require careful control of spatial uniformity (gas distribution and moisture gradients) and compatibility with structural schedules. While laboratory-scale results demonstrate the viability of the chemistry and the timing principle, field deployment must ensure that CO_2 delivery is sufficiently uniform across realistic thicknesses and that enclosure leakage and ambient exchange do not shift the carbonation pathway toward the constant-exposure failure mode. We view this as an engineering optimization problem rather than a fundamental scientific barrier: the absorption window can be targeted with controlled delivery, but it must be targeted consistently.

5.7. Summary of the Mechanistic Claims and What Remains to be Tested

The dynamic approach is most defensible when framed as controlled delivery aligned with hydration-driven changes in pore water accessibility and alkaline buffer stability. Early CO_2 promotes transient carbonate formation and nucleation seeding through dissolution–reprecipitation, whereas late or constant exposure shifts the system toward diffusion-limited surface carbonation, crust formation, and cracking. The proposed absorption window provides a unified framework linking kinetics (uptake enhancement), mineralogy (stage 2 nesquehonite and calcite), porosity refinement (capillary pore reduction), and performance (strength and pH retention). The method is currently bounded by MgO replacement levels ($\leq$ 30%) to avoid brucite-driven expansion. With suitable gas-enclosure logistics, the approach appears scalable for cast-in-place concrete, provided that temporal and spatial control are maintained to preserve the dynamic mineralization regime.

6. Conclusion

This study demonstrates that dynamic CO_2 absorption during concrete hydration can be engineered to increase both carbon retention and material performance, rather than treating carbonation as an uncontrolled after-effect of ambient exposure. When CO_2 was delivered within the hydration-stage window between initial set and final set, CO_2 uptake increased by approximately fourfold relative to constant exposure, reaching 18–22% uptake versus <5% under comparable cumulative conditions. In parallel, mechanical performance improved: 28-day compressive strength increased by 12% for dynamic samples (58 MPa) relative to the control (52 MPa), while constant high CO_2 exposure led to lower strength (43 MPa), consistent with diffusion restriction, surface crusting, and associated cracking. Microstructural measurements further supported a causal coupling between timed CO_2 delivery and pore refinement: mercury intrusion porosimetry indicated a substantial reduction in accessible pore size (median from 45 nm to 12 nm), attributable to carbonate filling of capillary pores. Importantly for durability-relevant chemistry, dynamic samples maintained pore-solution pH above 10.5 after 28 days, indicating that the approach can avoid passivation-loss risks associated with excessive alkalinity depletion.

From a theoretical standpoint, the results provide what is, to our knowledge, a first demonstration of hydration-stage-specific CO_2 reactivity as a tunable design variable. The central insight is that CO_2 reactivity is not only a function of cement composition and environmental availability; it is also governed by the temporal evolution of pore connectivity, ion availability (Ca^{2+}/Mg^{2+}), and the ability of carbonation products to dissolve–reprecipitate and seed nucleation. This reframes CO_2 absorption from a passive mineralization outcome into an active kinetic design parameter aligned with hydration. We further infer that early CO_2 promotes transient carbonate formation that can dissolve and reprecipitate to create nucleation sites, whereas late or constant exposure mainly carbonates already-formed C–S–H regions in a diffusion-limited regime that is mechanically less favorable.

Practically, the implications are straightforward but constrained by engineering requirements. The observed coupling suggests that precast concrete components can be engineered for carbon-negative pathways using relatively dilute CO_2 streams, provided that delivery is synchronized with curing and moisture state. With appropriate gas-enclosure strategies, the same logic may extend to in-situ elements, where temporary CO_2 tents could meter gas transport without requiring heavy infrastructure. However, the approach will remain formulation- and process-sensitive; for example, it operates reliably within a limited MgO replacement regime, where excessive Mg can drive brucite-related expansion.

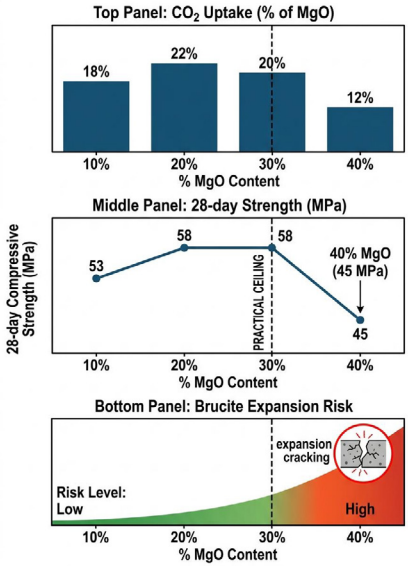

Figure 8: Effect of MgO Replacement Level (10–40%) on CO_2 Uptake, Strength, and Brucite Expansion Risk Under Dynamic Curing

Future work should prioritize system-level verification. A life cycle assessment (LCA) is needed to quantify net carbon benefit after accounting for CO_2 capture, transport, and any additional process inputs. Long-term durability must be tested under relevant stressors, including freeze–thaw cycling and chloride ingress, to confirm that carbonate-induced pore refinement does not introduce unexpected transport pathways or chemical instabilities. Finally, process optimization should include superplasticizer compatibility and rheology retention, since workability control during dynamic curing will be essential for scalable manufacturing.

References

1. Lothenbach, B., & Winnefeld, F. (2006). Thermodynamic modelling of the hydration of Portland cement. *Cement and Concrete Research, 36*(2), 209-226.
2. Galan, I., Glasser, F. P., & Andrade, C. (2015). Carbonation of concrete: A review of the mechanisms and factors affecting the process. *Cement and Concrete Composites, 63*, 1-11.
3. Morandeau, A., Thiery, M., & Dangla, P. (2014). Investigation of the carbonation mechanism of CH and CSH in terms of kinetics, microstructure changes and moisture properties. *Cement and concrete research, 56*, 153-170.
4. Vandeperre, L. J., & Al-Tabbaa, A. (2007). Accelerated carbonation of reactive MgO cements. *Advances in Cement Research, 19*(2), 67-79.
5. Unluer, C., & Al-Tabbaa, A. (2013). Characterization of light and heavy MgO products for carbonation. *Cement and Concrete Research, 45*, 49-58.
6. Mo, L., & Panesar, D. K. (2012). Effects of accelerated carbonation on the microstructure of reactive MgO cements. *Cement and Concrete Composites, 34*(6), 726-735.
7. Ruan, S., & Unluer, C. (2016). Comparative life cycle assessment of reactive MgO and Portland cement production. *Journal of Cleaner Production, 137*, 258-273.
8. Zhang, D., Ghouleh, Z., & Shao, Y. (2017). Review on carbonation curing of cement-based materials. *Journal of CO2 Utilization, 21*, 119-131.
9. Hidalgo, A., Andrade, C., & Alonso, C. (2012). Microstructural changes induced by carbonation in cement pastes. *Materials and Structures, 45*(1), 165-174.
10. Rostami, V., Shao, Y., & Boyd, A. J. (2011). Durability of concrete pipes subjected to combined steam and carbonation curing. Construction and Building Materials, 25(8), 3345-3355.
11. Monkman, S., & MacDonald, M. (2017). On the carbonation of cement-based materials: The role of CO_2 concentration and relative humidity. *Cement and Concrete Research, 92*, 11-19.
12. Pade, C., & Guimaraes, M. (2007). The CO2 uptake of concrete in a 100 year perspective. Cement and concrete research, 37(9), 1348-1356.
13. Sanjuan, M. Á., Andrade, C., & Mora, P. (2020). Carbonation of concrete and CO_2 sequestration: A review. *Applied Sciences, 10*(17), 5813.
14. De Schepper, M., Van den Heede, P., Van Driessche, I., & De Belie, N. (2014). Life cycle assessment of completely recyclable concrete. *Materials, 7*(8), 6010-6027.
15. Lothenbach, B., Matschei, T., & Glasser, F. P. (2015). Thermodynamic modelling of the effect of temperature on the hydration of Portland cement. *Cement and Concrete Research, 67*, 303-311.
16. Monkman, S., & Shao, Y. (2010). Carbonation curing of concrete: A review of the state of the art. *Journal of Materials in Civil Engineering, 22*(12), 1202-1210.
17. Xuan, D., Zhan, B., & Poon, C. S. (2016). Assessment of mechanical properties of concrete incorporating carbonated recycled concrete aggregates. *Cement and Concrete Composites, 65*, 67-74.
18. Shi, C., He, F., & Wu, Z. (2012). A review on carbonation curing of cement-based materials. *Journal of Wuhan University of Technology-Mater. Sci. Ed., 27*(6), 1037-1043.

19. Wang, D., Xiao, J., & Duan, Z. (2017). Performance of concrete prepared with carbonated recycled concrete aggregates. *Construction and Building Materials, 135*, 120-127.
20. Jang, J. G., Kim, G. M., & Lee, H. K. (2015). Review on recent advances in carbon dioxide utilization for cement-based materials. *KSCE Journal of Civil Engineering, 19*(7), 2011-2019.